Intertropical Convergence Zones during the Active Season in Daily Data

GUDRUN MAGNUSDOTTIR AND CHIA-CHI WANG

Department of Earth System Science, University of California, Irvine, Irvine, California

(Manuscript received 15 May 2007, in final form 11 December 2007)

ABSTRACT

Synoptic-scale variability of vorticity structures in the lower troposphere of the tropics is analyzed in 23 yr of daily averaged high-resolution reanalysis data. The vorticity structures can be divided into zonally elongated vorticity strips, classified as intertropical convergence zones (ITCZs), and more localized maxima, termed westward-propagating disturbances. A composite of such variability is presented for the east to central Pacific and for the east Atlantic/Africa region, both in summer. The composite in the east Pacific is zonally elongated and ITCZ-like, propagating westward over a number of days before dissipating. The spatial structure of the vorticity strip shows the characteristic cyclonic tilt into the latitudinal direction with time that is also seen in modeling experiments. The composite over the Atlantic/Africa region shows two active regions that are correlated on synoptic time scales. The disturbances in the southern region are better developed and longer lasting, even though the time and space scales are smaller than over the east Pacific. Overall, variability over the Atlantic is consistent with variability due to African easterly waves. The double ITCZ in spring in the east Pacific is different from the few earlier studies available. It is stronger south of the equator and located at 10°S, which is farther poleward than earlier studies have indicated. The northern branch that is weak in comparison is located at 5°N. The two branches of the double ITCZ tend to appear in tandem on the 2-week time scale.

1. Introduction

We are interested in synoptic (time scale of 2–25 days) variability of the intertropical convergence zone (ITCZ) and the closely associated westward-propagating disturbances (WPDs) during the active season in the eastern Pacific. The term WPD is taken to encompass the terms "tropical disturbance" and "tropical cyclone" as well as less-well-developed westward-propagating disturbances or easterly waves. Both the ITCZ and WPD have signatures of a local maximum in lower-tropospheric relative vorticity. The ITCZ has the signature of a zonally elongated vorticity strip, whereas the vorticity signature of WPDs is more axisymmetric in shape, especially for the stronger cases corresponding to an isolated vortex.

The close association between the east Pacific ITCZ and WPDs arises as the ITCZ goes through a number of stages during its life cycle, ending in breakdown into individual WPDs. The ITCZ stages include formation of the vorticity strip, undulations during the mature phase, and breakdown into WPDs, which may either grow into stronger systems while propagating away or dissipate. Sometimes ITCZ breakdown results in a number of weak WPD-type disturbances that continue their coherent westward propagation as they weaken further and finally dissipate. In these cases, we refer to the system as a dissipating ITCZ rather than individual WPDs. The ITCZ may also break down after interaction with a well-developed external WPD. In other cases a weak WPD (or an easterly wave) is seen propagating through the ITCZ without breakdown. The entire life cycle of ITCZ generation and breakdown may take anywhere from 2 days to 3 weeks. Wang and Magnusdottir (2006, hereafter WM06) detail ITCZ breakdown events in the east Pacific in May–October, which is the active season, using a variety of high horizontal resolution data sources that were available in 1999–2003. They classify the ITCZ breakdown events into those associated with interaction with an external WPD and those events that arose because of instability of the vorticity strip—the vortex rollup breakdown. Furthermore, they classify the breaking ITCZs into vertically

Corresponding author address: Gudrun Magnusdottir, Department of Earth System Science, University of California, Irvine, Irvine, CA 92697-3100.
E-mail: gudrun@uci.edu

DOI: 10.1175/2007JAS2518.1

deep and shallow systems because not all of the ITCZs are associated with deep convection (WM06). They find that ITCZ breakdown occurs with approximately the same frequency for each of the two breakdown mechanisms. They detect more numerous deep ITCZs and fewer shallow ones. From late summer to early fall the ITCZ is present much of the time. Generally, within a couple of days following breakdown, another ITCZ forms in the original location.

Our three-dimensional modeling study (Wang and Magnusdottir 2005) of ITCZ breakdown resulting from vortex rollup showed that a minimum horizontal resolution of T106 ($1.1° \times 1.1°$) is required to resolve the breakdown process. Nieto Ferreira and Schubert (1997) used a higher resolution in barotropic simulations of this process. Sobel and Bretherton (1999) were unable to find evidence of low-level vorticity strips in National Centers for Environmental Prediction–National Center for Atmospheric Research (NCEP–NCAR) reanalysis data, possibly because the horizontal resolution of the data is only T42 ($2.7° \times 2.7°$).

The ITCZ life cycle is highly variable in time, meaning that each of the identified stages is quite variable, in addition to differences in spatial characteristics among them. This means that traditional techniques in making composites are not applicable to the ITCZ and its breakdown. Here we use spectral techniques to isolate the signal of ITCZ and WPD variability in a rather long time series of high horizontal resolution reanalysis data, the 40-yr European Centre for Medium-Range Weather Forecasts (ECMWF) Re-Analysis (ERA-40) dataset.

Spectral methods have a long history in the analysis of tropical variability, especially for analyzing signatures of the convectively coupled equatorial modes (e.g., Takayabu 1994; Pires et al. 1997; Wheeler and Kiladis 1999, hereafter WK99). The earlier studies have therefore concentrated on the convective signatures, especially the outgoing longwave radiation (OLR) field that has the strongest signal in the upper troposphere. Here, we are interested in the lower tropospheric signature, which is most important in the early development of organized tropical systems. Both shallow and deep tropical systems have a lower tropospheric signature. Recently, the importance of shallow convection in the tropics has been highlighted in several observational studies (e.g., Zhang et al. 2004). This shallow component is captured by studying the signature in the lower tropospheric vorticity field, whereas it is largely lost in OLR.

Here we extend the analysis in WM06 by using only one source of data, but one that has a much longer time extent. We use the ERA-40 data (1979–2001), which are of high enough horizontal resolution to capture ITCZ breakdown events. We perform zonal wavenumber–frequency spectral analysis on the 850-hPa vorticity field, thereby focusing on rotational features in the tropical atmosphere such as WPDs and ITCZs. To focus on regional and seasonal characteristics, we perform the analysis only in the region and during the season of interest. Our primary motivation is to examine ITCZ (and WPD) variability in the area of the tropical east Pacific north of the equator during the summer half of the year when the ITCZ is frequently observed. We then go on to examine the tropical east Atlantic in summer, which is an active area and season for WPDs originating over Africa. Finally, we apply the method to the equatorial eastern Pacific in spring when a double ITCZ (on both sides of the equator) is often detected. The paper is organized as follows: section 2 describes the data and analysis; section 3 shows results from the eastern Pacific, north of the equator, during May–October; section 4 shows results for the eastern tropical Atlantic, north of the equator, during May–October; section 5 shows results for the eastern Pacific, symmetric about the equator, centered on the time when the double ITCZ has been observed in March and April; and section 6 contains concluding remarks.

2. Data, analysis, and global results

Daily averaged ERA-40 data are used over 23 yr, spanning 1979–2001. Although the ERA-40 dataset extends back to 1957, cloud motion winds from satellites were assimilated in ERA-40 starting in 1979. For the tropical ocean region where in situ observations are sparse it is essential to have these data included. We make use of the dataset that is archived at NCAR, which is of horizontal resolution T106.

We choose to use 850-hPa relative vorticity to represent tropical variability. Low-level relative vorticity represents synoptic-scale ITCZ and weak WPDs the best (e.g., WM06; Sobel and Bretherton 1999). In addition, the analysis scheme assimilates the cloud motion winds specifically at the 850-hPa level, making it most useful for our analysis. Most previous, more recent studies of variability in the tropics have made use of the OLR field. The OLR field is primarily an indicator of deep convection and is ideal for studying convectively coupled waves. However, we are looking for signatures of systems that may be less mature, or less vertically developed, than convectively coupled waves. At the same time, we need to include the signature of the deep systems. This is accomplished by using 850-hPa relative vorticity. Relative vorticity at 850 hPa better represents low-level cyclonic flow and convergence than OLR.

Also, relative vorticity is less noisy than convergence in daily data.

In a study over several recent years we found that the 975-hPa relative vorticity field in NCEP high-resolution tropospheric analysis is highly correlated with the vorticity field as computed from surface winds obtained from the Quick Scatterometer (QuikSCAT) satellite. The two fields were highly correlated (at least 0.7 for all points in the image when some vorticity structure was in the field of view) even before data from the satellite was assimilated into the analysis. The NCEP analysis product is only available from 1999, which is the main reason we decided to use ERA-40 data. The fidelity with which one product represents the low-level vorticity field gave us increased confidence in the ERA-40 lower-tropospheric vorticity field.

We broadly follow the analysis method in WK99, except that we apply their technique to the dynamical field of 850-hPa relative vorticity. The seasonal cycle is removed by removing the first three harmonics in time. The data are divided into 96-day windows, linearly tapering the end points to zero, while overlapping the windows by 2 months. A two-dimensional fast Fourier transform is performed on the zonal and time dimensions at each latitude. The resulting coefficients are summed over all latitudes of the domain to get the raw spectrum. We did not separate the spectrum into symmetric/antisymmetric parts about the equator. The significance test (F test) is done by dividing the raw spectrum by a background. The background spectrum is obtained from the raw spectrum by repeatedly applying 1–2–1 smoothing to it (WK99). The results are not sensitive to the exact method of smoothing that is performed to obtain the background.

Figure 1a shows the resulting spectrum (after dividing the raw spectrum by the background) summed over 0°–25°N, and Fig. 1b summed over 25°S–0° using global (all longitudes) data for May–October (inclusive). Negative (positive) wavenumbers indicate westward (eastward) propagation. The shaded area (values greater than 1.1) is where the spectrum is statistically significant at 95% confidence level with approximately 1000 degrees of freedom. The figure shows that almost the entire spectral signal (within our time scale of interest) is located in the Northern Hemisphere (NH), approximately following a line in the wavenumber–frequency diagram. The spectral signature in annual data (not shown) is similar in shape but much weaker. When we examined the 5 yr of 1999–2003 in detail in WM06, we found that in winter large-scale convective activity is associated with cold air surges from the extratropics. The tropical convection that is initiated typically connects to the extratropical system and moves eastward. The character of these tropical systems, often called "plumes," is different from the westward-propagating phenomena that we are examining here. Wintertime plumes are considerably less frequent than summertime ITCZs and WPDs. In what follows, we shall focus on the summer half-year (except in section 5).

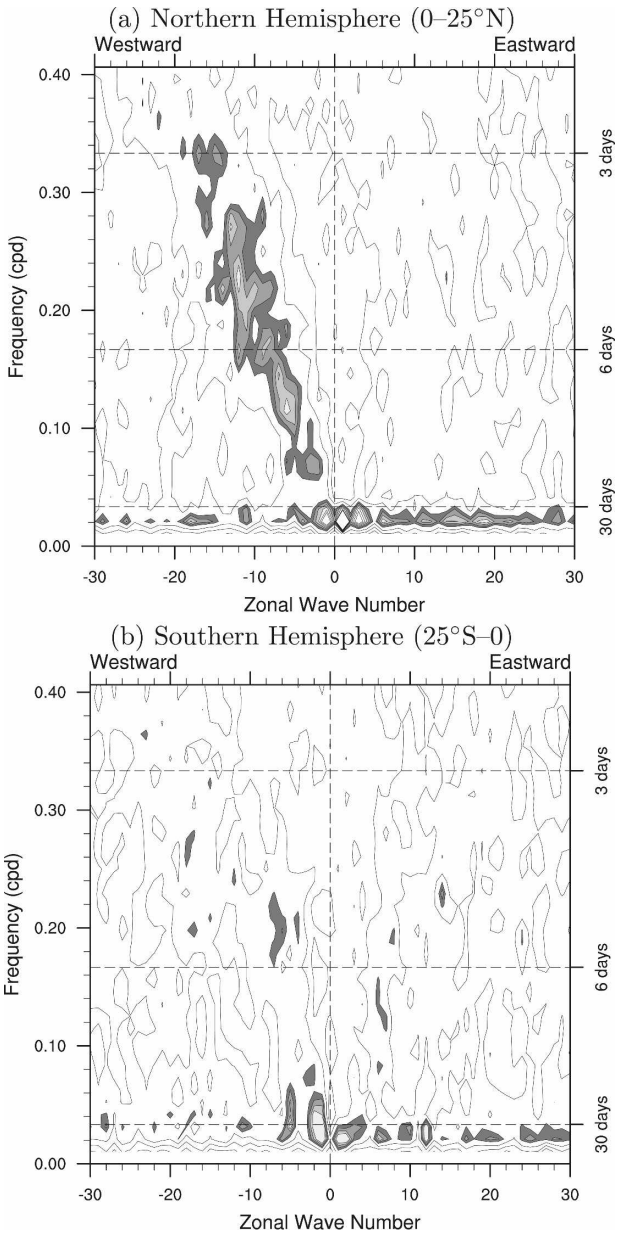

FIG. 1. The power spectrum (see text for details) using daily averaged 850-hPa relative vorticity, May–October 1979–2001 (inclusive) for the (a) Northern (equator to 25°N) and (b) Southern (equator to 25°S) Hemispheres. Contour interval is 0.1. Shading starts at 1.1.

We examined the spectral signal at each latitude point from the equator to 25°N (figures not shown) and

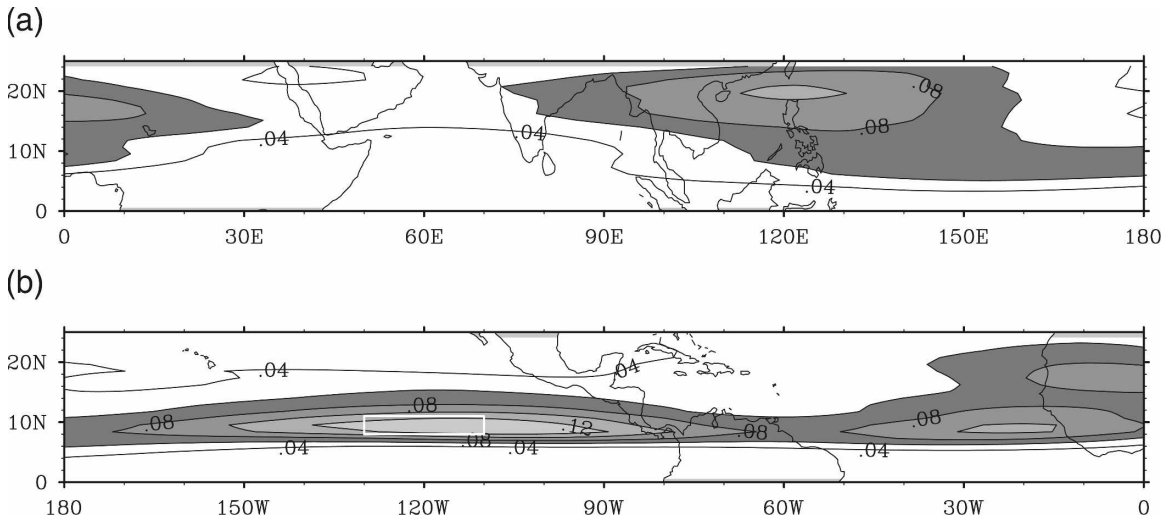

FIG. 2. Latitude, longitude plots of the variance of filtered 850-hPa vorticity for 0°–25°N, May–Oct 1979–2001 in the (a) Eastern and (b) Western Hemispheres. Contour interval is 0.02×10^{-10} s^{-2}. The white rectangle in the east Pacific shows the area over which we average the filtered vorticity to get the reference time series for regression analysis.

found that the spectral signal is negligible equatorward of 5°N. The location of the maximum spectral signal in the wavenumber–frequency plot is shifted gradually from low frequencies and low wavenumbers to higher frequencies and higher wavenumbers as the latitude is increased (to 25°N), approximately following the linear shape of the spectrum shown in Fig. 1a. This suggests that tropical activity has a longer time scale and a more zonally elongated spatial structure nearer the equator (still north of 5°N), while farther north shorter time scales and zonal structures prevail. This is consistent with earlier studies on tropical variability showing that ITCZ breakdown can lead to WPDs that have a northward component to their propagation.

Following WK99 we apply wavenumber–frequency filtering by extracting certain features from the spectrum. First, the box filter was chosen to extract the wavenumbers and frequencies where the spectrum is statistically significant at 95% confidence level or greater. The spatial distribution of the variance of the filtered vorticity, shown in Fig. 2, can be used to determine the geographical region associated with the spectral peaks. The area with the highest variance is an elongated zonal stretch in the eastern Pacific at approximately 10°N. This area clearly corresponds to the ITCZ and associated WPDs. A secondary zonal stretch of high variance is visible in the Atlantic. The Atlantic variance pattern has a secondary maximum at approximately 17°N, located mostly over Africa. The Atlantic/African region is an active area for African easterly waves (AEWs). In the Eastern Hemisphere the area of maximum variance is quite broad in latitude and corresponds to activities associated with the Asian summer monsoon.

Now that we have established that a zonally elongated and latitudinally limited area of maximum variance shows up prominently in summer, both in the east Pacific and the east Atlantic, we further isolate regions of interest. We can focus on certain longitudinal regions by setting the 850-hPa vorticity field to zero outside the region of interest while linearly tapering the edges to zero. We then apply the wavenumber–frequency spectral analysis to this reduced field. Two regions of interest corresponding to regions of maximum variance are isolated in summer. They are the eastern Pacific, at 5°–20°N, 180°–80°W, and the eastern Atlantic, extending over Africa at 5°–25°N, 60°W–10°E. Additionally, we considered one additional region in spring (mid-February to mid-May). This is the region of the east Pacific where a double ITCZ (on both sides of the equator) is frequently observed in March–April. This region extends from 140° to 60°W and from 15°S to 15°N.

We use cross-spectral analysis (von Storch and Zwiers 1999, their section 11.4) in sections 4 and 5 to examine if there are coherent features between latitudinal subregions—first, between regions on both sides of the African easterly jet (section 4), and second between features north and south of the equator in the east Pacific in spring (section 5).

3. Eastern Pacific, north of the equator

We are particularly interested in establishing a composite of ITCZ behavior in the tropical east Pacific

north of the equator. This is the region where we found active ITCZ evolution and breakdown on the synoptic time scale for the five summer half-years of 1999–2003 (WM06).

a. Wavenumber–frequency diagram

Figure 3 shows the power spectrum, divided by a background spectrum, of 850-hPa vorticity for May–October 1979–2001 for the 5°–20°N, 180°–80°W area. Again, the statistically significant part of the spectrum at less than monthly time scale is westward propagating and approximately aligns itself along the straight, dashed lines shown. The phase speed corresponding to this spectral signature is approximately $c = -8\ \mathrm{m\ s^{-1}}$. The other two sets of bold contours in the diagram indicate the dispersion curves for the $n = 1$ Rossby wave in a background state of rest (dotted) and in a background easterly flow $u = -2.6\ \mathrm{m\ s^{-1}}$, which is the area average (solid contours), for equivalent depths of 35, 70, and 150 m. The bold dashed lines along which the spectrum aligns itself indicate the corresponding Rossby wave under the longwave approximation.

Under the longwave approximation (e.g., Stevens et al. 1990), dispersive equatorial Rossby waves are approximated by nondispersive waves that have the zonal phase speed of the long (small zonal wavenumber) and low-frequency Rossby waves for all wavenumbers and frequencies. This corresponds to a scaling of length that has the zonal scale of variations greatly exceeding the meridional scale of variations, which of course is highly relevant to the ITCZ. The longwave approximation is obviously quite severe at wavenumbers greater than approximately 10, even while taking the background flow into account (see Fig. 3).

The spectral signature seen in Fig. 3 approximately corresponds to the tropical depression (TD) band found in a number of studies, including WK99. It does not correspond to any single normal mode on the equatorial β plane (Matsuno 1966). When we performed the same type of analysis as before, except on the pressure field at 850 hPa, we recovered close to the equatorial β-plane normal modes, such as those WK99 obtained from OLR data. In particular, both the Kelvin wave and the mixed Rossby–gravity (MRG) wave showed up prominently in the pressure field (not shown). The signature corresponding to the one seen in Fig. 3 was of secondary importance in terms of pressure. This approximately corresponds to the TD band and it is considerably weaker (not statistically significant) in pressure than in vorticity. Both the Kelvin wave and MRG wave (at low wavenumbers) are gravity-type waves, and one expects them to be of secondary importance for the rotational part of the flow. Likewise, one expects to see their signature prominently in the mass field (such as pressure).

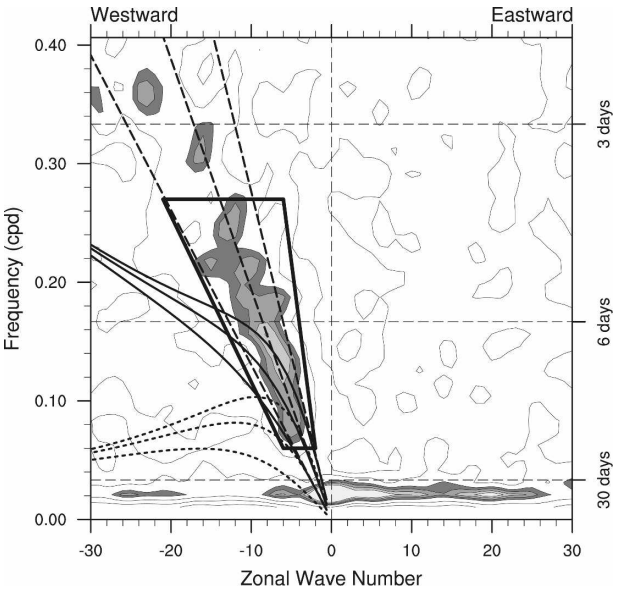

FIG. 3. The power spectrum of 850-hPa relative vorticity obtained using May–October 1979–2001 data for the tropical northeastern Pacific only (5°–20°N, 180°–80°W). Contour interval is 0.1 below 1.1 and 0.05 above 1.1. Shading starts at 1.1. Areas where the spectrum is statistically significant at the 95% confidence level are shaded. The box shows the filter (see text for details). The two sets of bold contours indicate the dispersion curves for the $n = 1$ Rossby wave in a background state of rest (dotted) and in a background easterly flow ($u = -2.6\ \mathrm{m\ s^{-1}}$, which is the time mean, area average; solid contours) for equivalent depths of 35, 70, and 150 m. The bold dashed lines indicate the corresponding Rossby wave under the longwave approximation.

b. Composite of ITCZ

To form a composite of ITCZ behavior, we defined a box filter in the wavenumber–frequency diagram to extract the statistically significant signal for the time scales of interest. The filter is shown as the solid box in Fig. 3. We then computed the variance of the filtered vorticity. The spatial pattern of the variance is quite close to the variance using global data (all longitudes) in Fig. 2 except that the signal is isolated to the Pacific, east of the date line (not shown). The average variance over a zonally elongated rectangular area surrounding the point of maximum variance at 9.5°N, 120°W is chosen as the reference value for regression analysis. The rectangular area extends over 8°–11°N, 130°–110°W and is shown by the white box in Fig. 2. The time series of the filtered vorticity averaged over this rectangle is used to construct an index, which determines active

periods. Figure 4 shows the 25-day[1] running variance (curve) and the long-term variance (horizontal line) in the reference area for 1979–2001 (x axis). The active periods are those that have the running variance greater than the long-term variance. The ITCZ index is defined as the area average of the vorticity value during active periods. Outside of active periods, this index is not considered and is set to missing value. From Fig. 4 we see that there is considerable interannual variability in active periods. Also, the active periods take place during the summer half-year only, consistent with WM06. We have done the same analysis using annual data for all 23 yr (not shown) and found no active periods outside of the summer half-year.

Using the index of tropical activity that is described above, we can project other fields onto it to extract the signal related to the tropical activity under examination. We do this by regression between the field and the index. At each grid point, we do a regression of the relative vorticity at 850 hPa against the index. Then, the regression equations are mapped together by using twice the standard deviation of the index as the independent variable. This value is chosen so that the magnitude of the index is comparable to the magnitude of vorticity observed in the east Pacific ITCZ in summer. Wheeler et al. (2000) also chose twice the standard deviation of an OLR index for a regression analysis that was meant to isolate the signature of the Kelvin and MRG waves. Regression with different time lags provides the composite of the time evolution of tropical activity in which we are interested.

Figure 5 shows the composite of ITCZ time evolution from lag −5 days to +6 days. The figure shows the formation of the ITCZ stretching westward from the coast of Central America and centered around 90°W (at lag −5 day). The vorticity strip (the ITCZ) gradually extends westward with time and increases in value until it reaches its maximum strength (at a single point) on day −1. After day −1, the vorticity strip propagates westward with slightly decreasing maximum strength. The ITCZ not only propagates westward, but also tilts cyclonically with time. We have seen this cyclonic tilt both in our numerical simulations (Wang and Magnusdottir 2005) and observations (WM06); it arises because of the vorticity strip's induced velocity field, which acts to advect the strip, and this leads to a tilt (in the latitudinal direction) of the strip with time. The tilt is resisted by the β effect, but it is still evident. Associated with the induced velocity field is the advection of negative vorticity from the other hemisphere, which is also seen in numerical simulations. The time evolution of the vorticity strip that is described here shows a typical ITCZ life cycle from formation to dissipation. The methodology does not allow us to depict WPDs per se because they are much more random than the ITCZ both in space and time. However, the set of composite maps does show the weakening of the ITCZ with time as well as a clear westward propagation and the tilting of the long axis of the composited vorticity strip.

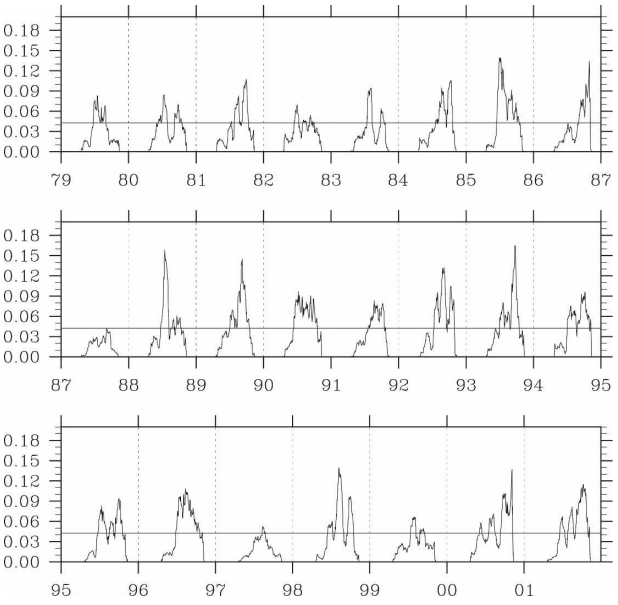

FIG. 4. The 25-day running variance (curve) of filtered relative vorticity over the reference area (rectangle in Fig. 2) and the variance over the entire time series of filtered vorticity in the reference area (horizontal line). The periods whose running variance is greater than the long-term variance are defined as active periods. The y axis is variance in 1×10^{-10} s^{-2}; the x axis is time from January 1979–December 2001 (inclusive).

The above composite picture is not sensitive to the exact method of defining the reference value for variance of vorticity. We tried simply using the maximum value of vorticity variance as well as averages over slightly different regions that included the maximum value. The different reference values resulted in very similar composite pictures. They did, however, result in slightly different interannual variability of the running variance. We note in passing that the running variance in Fig. 4 is quite small during the strong ENSO events during the summers of 1982, 1987, and 1997. This implies that the warm sea surface temperature (SST) in the equatorial central Pacific associated with strong ENSO events goes hand in hand with decreased tropical variability on synoptic time scales (up to 25 days) in

[1] The number, 25 days, is chosen from the longest time scale of the box filter. For other regions, this number is chosen accordingly.

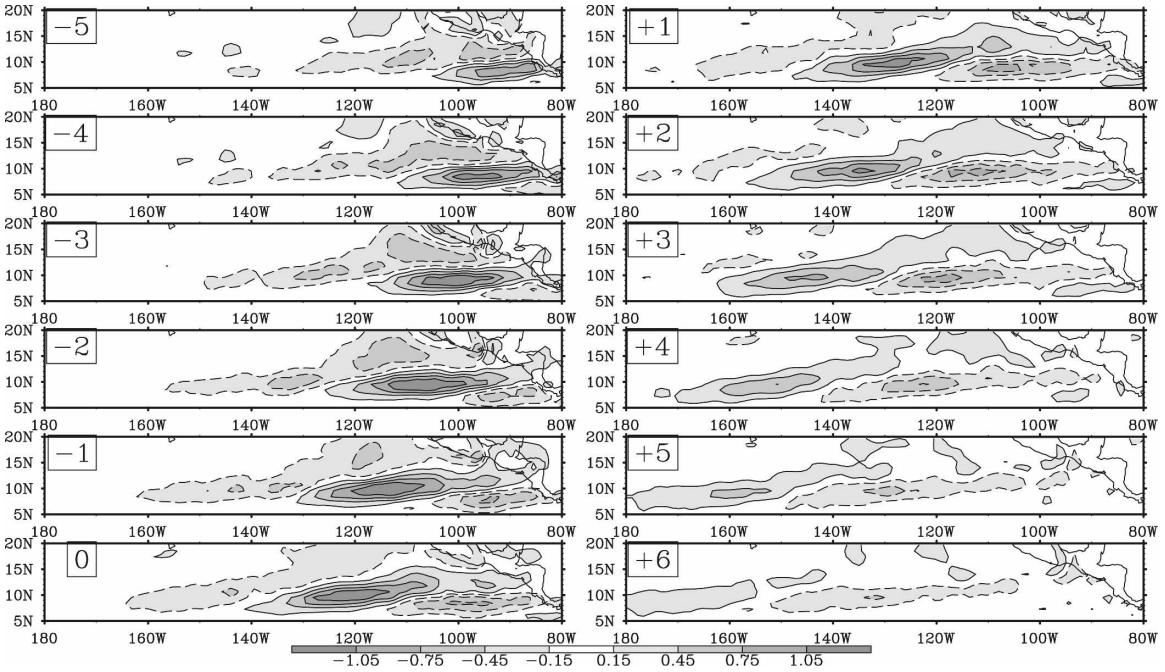

FIG. 5. Composite of the filtered vorticity anomaly at 850 hPa in the east Pacific in May–October 1979–2001. The lag/lead is indicated in each frame, from −5 to +6 days. Contour interval is 0.5×10^{-5} s^{-1}. Shaded areas have values greater/smaller than $\pm 0.25 \times 10^{-5}$ s^{-1}.

the latitude range of 5°–20°N. The warming of equatorial SST may be associated with an equatorward shift in the location of ITCZs and/or it may lead to weaker WPDs that form as a result of ITCZ breakdown.

4. The Atlantic, north of the equator

The tropical Atlantic in summer on the 2–25-day time scale is dominated by AEWs that originate over the African continent. A well-defined zonally elongated vorticity strip (the ITCZ) is not as prevalent over the Atlantic on these time scales as it is over the east Pacific. However, Agee (1972) reported an incident of tropical cyclogenesis in the region arising from instability of the ITCZ. The variance map of filtered 850-hPa vorticity from global data in summer (Fig. 2) shows a double maximum in the region. We limit the area of interest in this case to 5°–25°N, 60°W–10°E. Figure 6 shows the power spectrum that is obtained by setting the 850 vorticity to zero outside the area of interest and tapering the zonal edges to zero. Even though many features of the spectrum are similar to the one in the eastern Pacific (Fig. 3), note that in this case the maximum spectrum is located at higher frequencies (and wavenumbers), from about 2.5 to 7.5 per day. This shows that tropical synoptic activity in the Atlantic basin and over West Africa has a shorter time scale, which is consistent with the region being dominated by AEWs. In Fig. 6 we have drawn in the filter that we use and Fig. 7 shows the corresponding variance map. It shows that even though we neglect data outside of a fairly restricted longitude range, the important parts of the map, such as the well-separated double maximum,

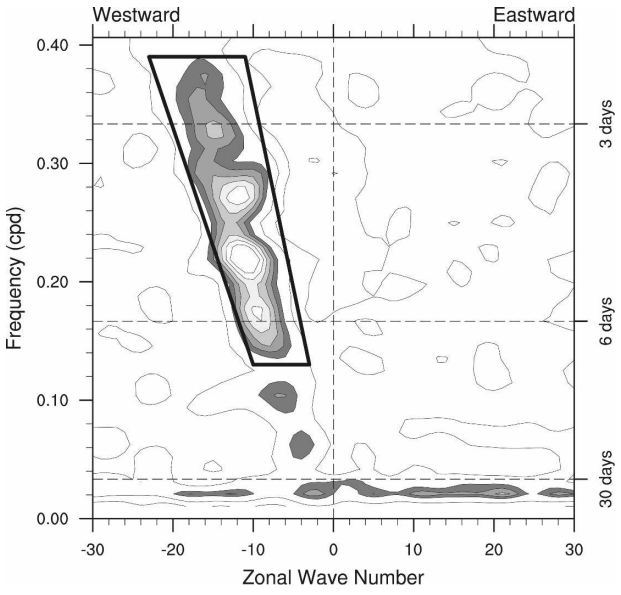

FIG. 6. Same as Fig. 3, but for the region from the tropical eastern Atlantic to western Africa (5°–25°N, 60°W–10°E).

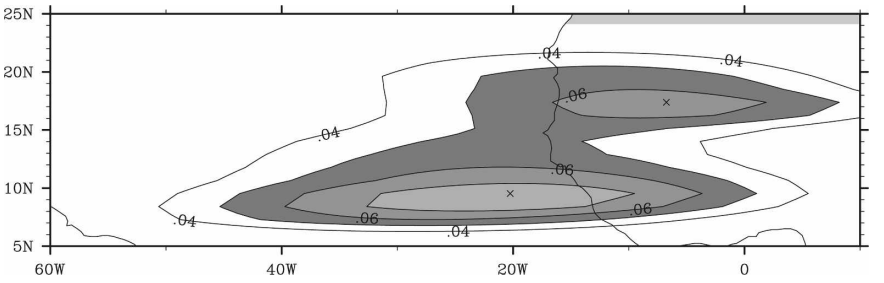

FIG. 7. Same as Fig. 2, but for the tropical northeastern Atlantic to western Africa. This figure shows two local variance maxima at (9.5°N, 20.5°W) and (17.4°N, 7°W). The contour interval is 0.01×10^{-10} s^{-2}.

remain. This double-maximum pattern does not show up in OLR data (e.g., Kiladis et al. 2006) because the northern disturbances do not have an OLR signature.

Many previous studies have remarked on the two storm tracks over Africa on each side of the African easterly jet (e.g., Nitta and Takayabu 1985; Pytharoulis and Thorncroft 1999; Fink and Reiner 2003). These studies have found that disturbances on each track are closely related. The two tracks appear to merge into the southern track over the east Atlantic close to the African coast (Thorncroft and Hodges 2001; Fink et al. 2004). To consider each of the tracks separately, we computed the spectrum for each of two subregions that were defined by latitude range. Figures 8a,b show the spectrum for the southern (5°–15°N) and the northern (15°–25°N) regions, respectively. For the southern region that has vorticity variance extending in a narrow zone over the Atlantic, there is statistically significant power at time scales up to 20 days. The area-averaged mean zonal flow in the southern region is $u = -4.5$ m s^{-1} and about half that value in the northern region. The phase speed corresponding to the shape of the spectrum is approximately $c = -11$ m s^{-1} in the southern region and $c = -8$ m s^{-1} in the northern region where the power is concentrated at time scales less than 8 days (Fig. 8b).

We carried out two composite studies (lead/lag correlation maps) of filtered vorticity,[2] using the points corresponding to maximum variance in each region as base points. The results are shown in Figs. 9a,b for the southern and northern Atlantic regions, respectively. In both figures the base point is indicated by ×. The southern disturbances are well developed at 2 days' lead time, reach maximum amplitude 1 day before reaching the base point, and then continue propagating zonally along 10°N out over the Atlantic where they appear to slowly dissipate. The northern disturbances have a

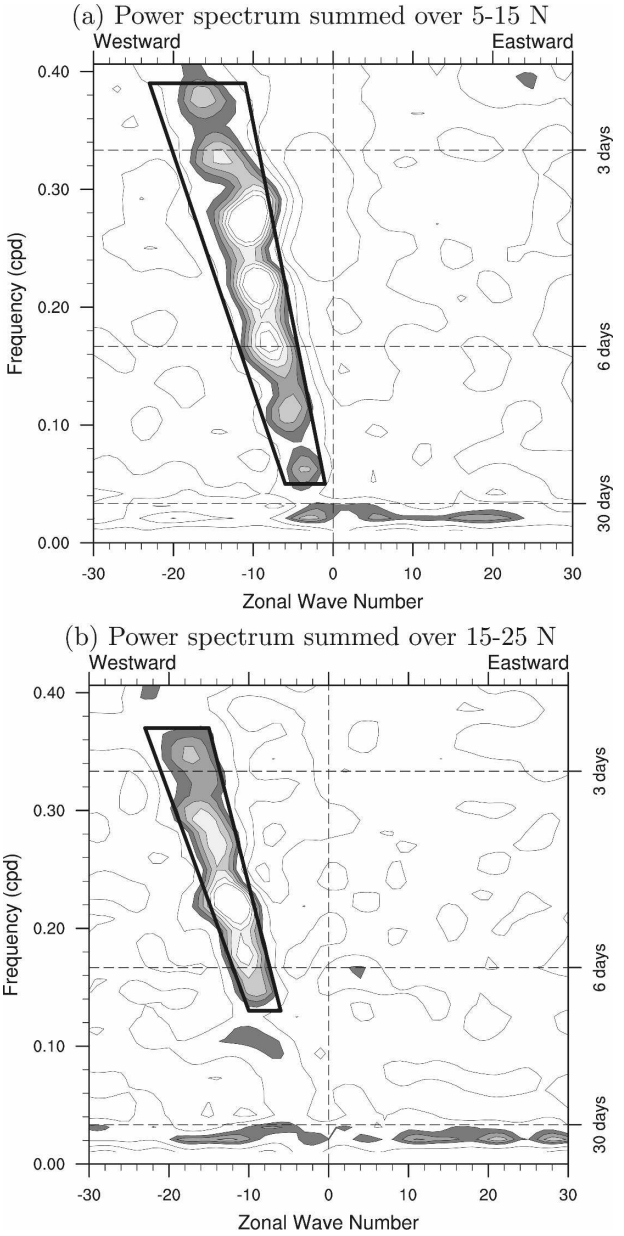

FIG. 8. Same as Fig. 6, but for the two subregions (a) 5°–15°N, 60°W–10°E, and (b) 15°–25°N, 60°W–10°E.

[2] The box filters are shown in Figs. 8a–b.

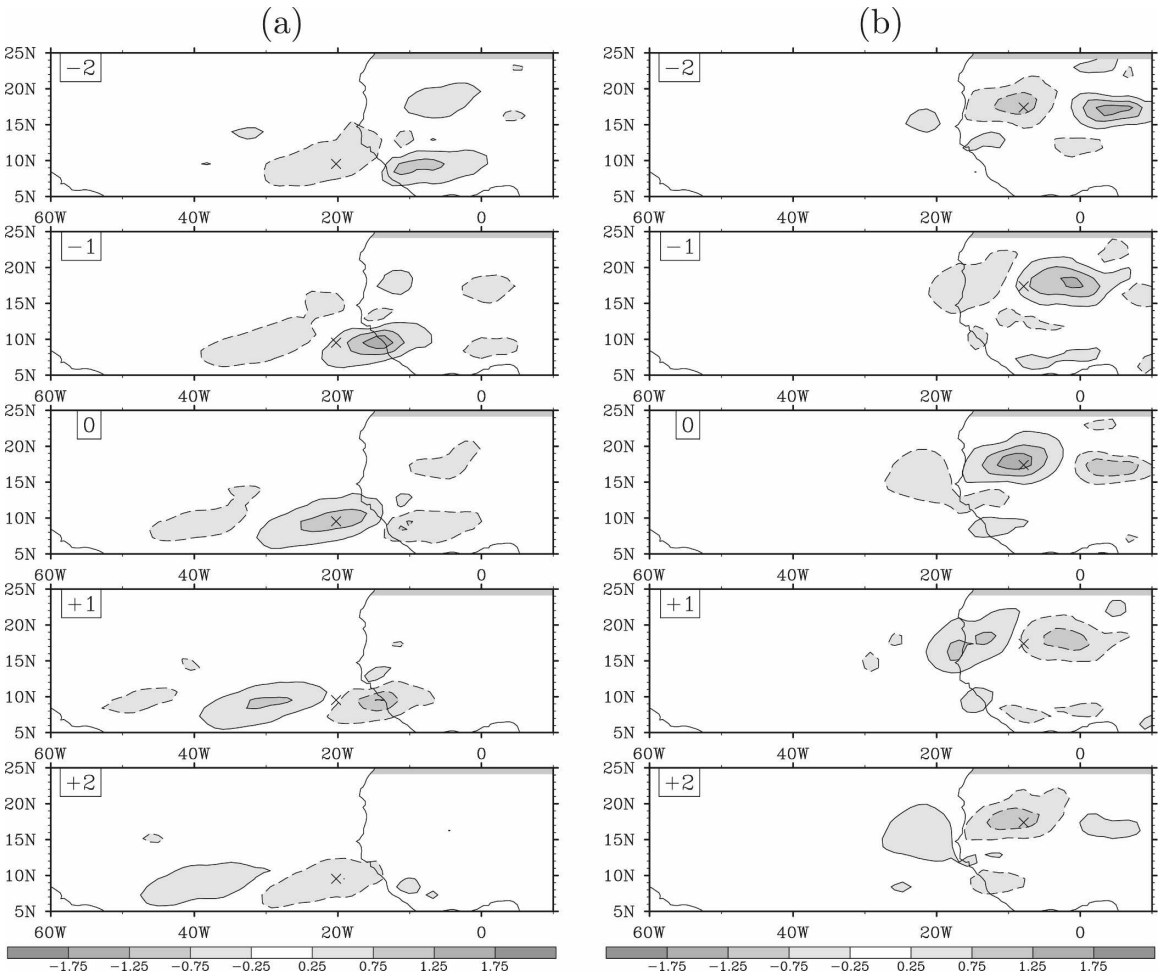

FIG. 9. Same as Fig. 5, but for African easterly waves in the (a) southern and (b) northern regions.

strong signature at 2–0-days' lead along 17°N, and then appear to turn equatorward and dissipate. This is consistent with these disturbances being largely dry and driven by baroclinic instability of the jet, which results from differential heating over the African continent. As the disturbances leave the continent they lose their driving support and start dissipating. Note that the vorticity structures along the northern track do not develop the cyclonic tilt that is characteristic of vorticity strips in the NH (Wang and Magnusdottir 2005). Even though the vorticity structures along the southern track appear to develop a slight tilt, the composite appears wavelike. Thus, in accordance with previous studies, the disturbances in this region are dominated by AEWs.

We performed a cross-spectral analysis to investigate the coherence between the northern and southern disturbances. Figure 10 shows the coherence squared and the phase difference between the disturbances in the two areas. The coherence squared is only contoured where it is statistically significant at 95% confidence level (based on 300 degrees of freedom). The two types of disturbances show strong coherence for westward-propagating waves of the 3–5-day time scale. They are mostly in phase (arrows pointing to the right) for the higher-frequency, shorter waves, gradually showing more phase difference (arrows turn counterclockwise) when the scales increase. This is entirely consistent with previous studies and lends credence to our analysis of disturbances in the eastern Pacific, which by comparison are poorly documented on the synoptic time scale.

5. Eastern Pacific in spring for both sides of the equator

At certain times and in certain locations, two ITCZs have been observed on both sides of the equator in the same longitudinal region. This phenomenon has been called the double ITCZ. In the eastern Pacific the double ITCZ is prevalent during March–April in non–

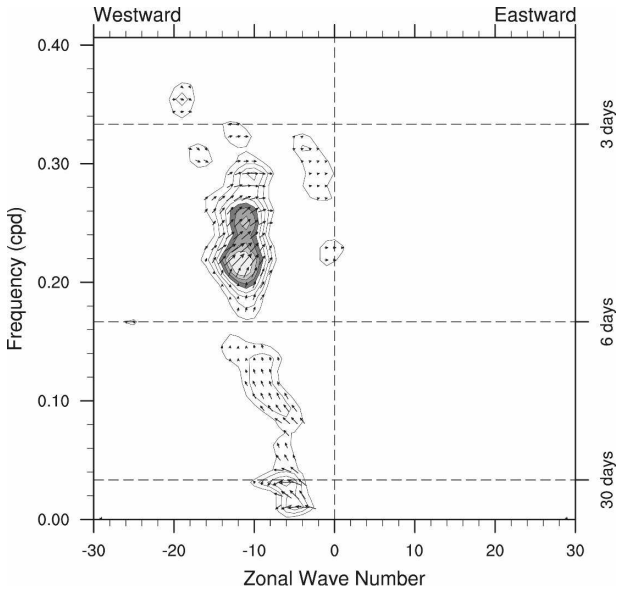

FIG. 10. Coherence squared (contours) and phase difference (arrows) between north and south AEWs. Contours and arrows are plotted where the coherence squared is statistically significant at the 95% confidence level (value greater than 0.02). Arrows pointing to the right correspond to disturbances that are in phase.

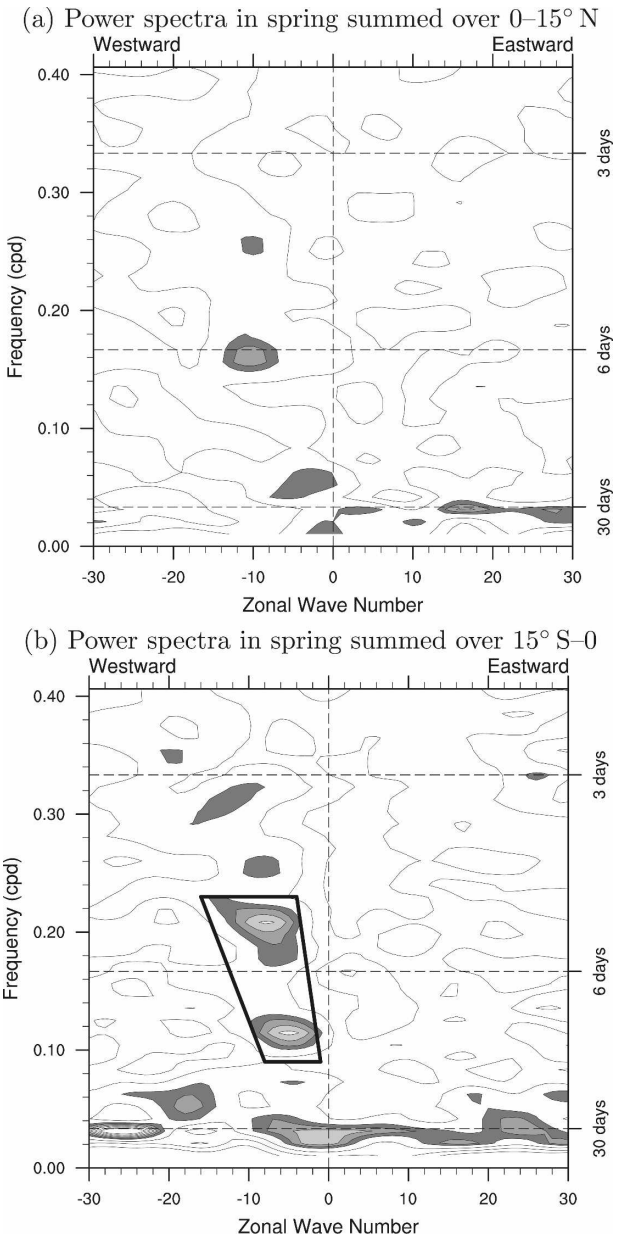

FIG. 11. Same as Fig. 3, but for spring and the regions are limited to (a) 0°–15°N, 140°–60°W and (b) 15°S–0°, 140°–60°W.

El Niño years. It has been observed to appear as early as late February and last as long as early May (Lietzke et al. 2001). Very few studies have dealt with the double ITCZ and all have focused on time averages over a month. Only Lietzke et al. (2001) and Gu et al. (2005) examine weekly averages as well, however, over only very few years of data. It is entirely unclear what the behavior is on synoptic time scales as represented in 850-hPa vorticity in ERA-40 data.

We chose to focus the analysis on the time period from mid-February to mid-May. We picked longitudes 140°–80°W as the area of interest to avoid the southern Pacific convergence zone, which at times extends eastward beyond the date line. Each side of the equator is treated separately because the two regions may act differently. Latitudes from the equator to 15°N and S were chosen. Figure 11 shows the power spectra for the two regions. The signal is considerably weaker than before (Figs. 3, 6, 8), especially the NH signal (Fig. 11a). The Southern Hemispheric part that has more power (Fig. 11b) also shows alignment in the diagram corresponding to disturbances of faster phase speeds, $c = -11$ m s^{-1}. For comparison, the area-averaged mean zonal flow in the southern region is $u = -4.7$ m s^{-1}.

The lead/lag correlation map of filtered vorticity for the region south of the equator is shown in Fig. 12, where we apply the box filter shown in Fig. 11b. The base point for the regression at 10°S, 121°W is indicated by $\times$ and corresponds to the point of maximum variance. (Note that in the Southern Hemisphere a cyclonic circulation feature is associated with a negative relative vorticity field.) The composite reveals a zonally elongated negative vorticity structure that develops an anticyclonic tilt with time as seen in Fig. 12 on day 0. The x axis of the composite vorticity shows a slight cyclonic tilt in the NH (not shown). This was also seen during the summer half-year in this location and in the southern track over the Atlantic. This is entirely consistent with the tilt seen in our 3D simulations of a heating-

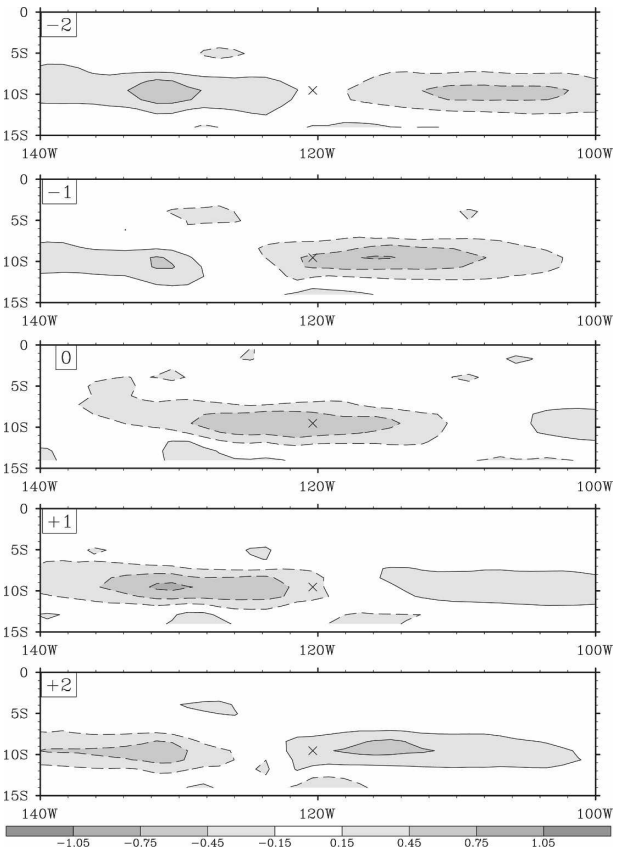

FIG. 12. Same as Fig. 5, but for the southern branch (negative relative vorticity) of the double ITCZ in spring.

generated lower-tropospheric vorticity strip (Wang and Magnusdottir 2005). The NH point of maximum variance is at 5°N, 120°W (not shown); thus, the Northern and Southern Hemispheric base points are almost collocated in longitude but are at different latitudinal distance from the equator. Previous studies (e.g., Liu and Xie 2002) have located each branch of the spring double ITCZ in the east Pacific at approximately 5°N and S latitude.

It is of interest to examine the relationship between the spectra in the two regions of the double ITCZ. We performed cross-spectral analysis as before and found coherence between the two hemispheres on the time scale of about 2 weeks (not shown). The arrows, indicating phase difference, point to the left, meaning that the two branches of the ITCZ are in phase because relative vorticity is antisymmetric about the equator. Thus, we find that the two branches of the double ITCZ tend to appear together on the 2-week time scale. We are not aware of any other studies that have examined the double ITCZ in daily data. Gu et al. (2005) found that in monthly averaged rainfall there is competition between the two branches of the double ITCZ such that when one is strong the other is weak. Because we are using daily data we cannot comment on the longer time averages. Some might argue that the criterion of using the lower-tropospheric vorticity strip to define the ITCZ would include both shallow and deep structures, whereas the rainfall criterion would only include deep structures. This may be the case in some instances, however, early results from Cloudsat show precipitation resulting from shallow as well as deep systems (G. Stephens 2007, personal communications). More than anything the current results underscore the importance of examining the double ITCZ on shorter time scales than has previously been done.

The issue of a double ITCZ in the east Pacific presents a challenging problem to coupled climate models. The double ITCZ is only visible in observations in boreal spring, but it is present in many climate models yearlong (e.g., De Szoeke and Xie 2008; their Fig. 3). The double ITCZ has been found to exist in many climate models even when the equatorial SST cold tongue is not strong, pointing to an atmosphere-only mechanism.

6. Concluding remarks

We have presented a composite picture of the ITCZ on synoptic time scales in the east to central Pacific (Fig. 5) during the active season. According to this composite, the ITCZ builds from the easternmost part of the basin westward while propagating and eventually dissipating. The breakdown stage is not represented in the composite; rather the entire structure dissolves while tilting, and the trailing part recedes farther away from the equator.

Two additional regions were considered—the Atlantic, which in summer is dominated by WPDs, and the east Pacific in spring on both sides of the equator. The composite for the northern subregion of Atlantic/Africa is very different from the ITCZ composite. The time scale is shorter, the spatial pattern is more symmetric, and there is no tilt to the structure. Even though there is some tilt to the spatial pattern in the southern Atlantic region, it appears wavelike, with a considerably smaller spatial scale and a shorter time scale than in the Pacific. This corresponds to the prevalence of AEWs or WPDs in this region. In spring in the east Pacific, synoptic-scale variability is stronger in the Southern Hemisphere and it is located further away from the equator than in the NH. The corresponding composite reveals a zonally extended westward-propagating structure with the characteristic tilt of an ITCZ. The two branches of the double ITCZ tend to appear in tandem on the 2-week time scale.

The spectral signature of the ITCZ cannot be sepa-

rated from that of WPDs, rather both appear to correspond to what has previously been loosely termed the TD band. This signature is most prominent in lower tropospheric relative vorticity, and is secondary in pressure and OLR. The ITCZ/WPD band approximately follows lines in the wavenumber–frequency diagram, a fact that prompted us to reconsider the longwave approximation to the equatorial β-plane Rossby wave. This may be useful in areas dominated by ITCZ activity because of the spatial scaling implicit in the longwave approximation. Background easterly flow is shown to tilt the dispersive Rossby wave in the wavenumber–frequency diagram, but it does not account for the near-linear appearance of the spectrum. Also, the phase speed corresponding to the spectrum always far exceeds what we might identify as the background flow. Even though recent studies concentrating on only deep structures have been successful in relating tropical activity to normal modes, it is likely that the spectral signature that we observe in lower-tropospheric vorticity is due to a Rossby wave packet rather than an individual normal mode.

Acknowledgments. We thank Padhraic Smyth, Hal Stern, and Lucas Scharenbroich for valuable discussions during the course of this work, and George Kiladis for suggestions during the earliest stages. We thank Chidong Zhang, Adam Sobel, and an anonymous reviewer for carefully reviewing an earlier version of the manuscript. This work was supported by NSF Grant ATM0530926.

REFERENCES

Agee, E. M., 1972: Note on ITCZ wave disturbances and formation of tropical storm Anna. *Mon. Wea. Rev.,* **100,** 733–737.

De Szoeke, S. P., and S. P. Xie, 2008: The tropical eastern Pacific seasonal cycle: Assessment of errors and mechanisms in IPCC AR4 coupled ocean–atmosphere general circulation models. *J. Climate,* **21,** 2573–2590.

Fink, A. H., and A. Reiner, 2003: Spatiotemporal variability of the relation between African Easterly Waves and West African squall lines in 1998 and 1999. *J. Geophys. Res.,* **108,** 4332, doi:10.1029/2002JD002816.

——, D. G. Vincent, P. M. Reiner, and P. Speth, 2004: Mean state and wave disturbances during Phases I, II, and III of GATE based on ERA-40. *Mon. Wea. Rev.,* **132,** 1661–1683.

Gu, G., R. F. Adler, and A. H. Sobel, 2005: The eastern Pacific ITCZ during the boreal spring. *J. Atmos. Sci.,* **62,** 1157–1174.

Kiladis, G. N., C. D. Thorncroft, and N. M. J. Hall, 2006: Three-dimensional structure and dynamics of African easterly waves. *J. Atmos. Sci.,* **63,** 2212–2230.

Lietzke, C. E., C. Deser, and T. H. Vonder Haar, 2001: Evolutionary structure of the eastern Pacific double ITCZ based on satellite moisture profile retrievals. *J. Climate,* **14,** 743–751.

Liu, W. T., and X. Xie, 2002: Double intertropical convergence zones—A new look using scatterometer. *Geophys. Res. Lett.,* **29,** 2072, doi:10.1029/2002GL015431.

Matsuno, T., 1966: Quasi-geostrophic motions in the equatorial area. *J. Meteor. Soc. Japan,* **44,** 25–42.

Nieto Ferreira, R., and W. H. Schubert, 1997: Barotropic aspects of ITCZ breakdown. *J. Atmos. Sci.,* **54,** 261–285.

Nitta, T., and Y. Takayabu, 1985: Global analysis of the lower tropospheric disturbances in the tropics during the northern summer of the FGGE year. Part II: Regional characteristics of the disturbances. *Pure Appl. Geophys.,* **123,** 272–292.

Pires, P., J.-L. Redelsperger, and J.-P. Lafore, 1997: Equatorial atmospheric waves and their association to convection. *Mon. Wea. Rev.,* **125,** 1167–1184.

Pytharoulis, I., and C. D. Thorncroft, 1999: The low-level structure of African easterly waves in 1995. *Mon. Wea. Rev.,* **127,** 2266–2280.

Sobel, A. H., and C. S. Bretherton, 1999: Development of synoptic-scale disturbances over the summertime tropical northwest Pacific. *J. Atmos. Sci.,* **56,** 3106–3127.

Stevens, D. E., H. C. Kuo, W. H. Schubert, and P. E. Ciesielski, 1990: Quasi-balanced dynamics in the tropics. *J. Atmos. Sci.,* **47,** 2262–2273.

Takayabu, Y. N., 1994: Large scale cloud disturbances associated with equatorial waves. Part I: Spectral features of the cloud disturbances. *J. Meteor. Soc. Japan,* **72,** 433–449.

Thorncroft, C. D., and K. Hodges, 2001: African easterly wave variability and its relationship to Atlantic tropical cyclone activity. *J. Climate,* **14,** 1166–1179.

von Storch, H., and F. W. Zwiers, 1999: *Statistical Analysis in Climate Research.* Cambridge University Press, 499 pp.

Wang, C.-C., and G. Magnusdottir, 2005: ITCZ breakdown in three-dimensional flows. *J. Atmos. Sci.,* **62,** 1497–1512.

——, and ——, 2006: The ITCZ in the central and eastern Pacific on synoptic time scales. *Mon. Wea. Rev.,* **134,** 1405–1421.

Wheeler, M., and G. N. Kiladis, 1999: Convectively coupled equatorial waves: Analysis of clouds and temperature in the wavenumber–frequency domain. *J. Atmos. Sci.,* **56,** 374–399.

——, ——, and P. J. Webster, 2000: Large-scale dynamical fields associated with convectively coupled equatorial waves. *J. Atmos. Sci.,* **57,** 613–640.

Zhang, C., M. McGauley, and N. A. Bond, 2004: Shallow meridional circulation in the tropical Eastern Pacific. *J. Climate,* **17,** 133–139.